2-10-2016

Influence of RTIL Nanodomains on the Voltammetry and Spectroelectrochemistry Of Fullerene C_{60} in Benzonitrile/Room Temperature Ionic Liquids Mixtures

Abderrahman Atifi
Marquette University

Michael D. Ryan
Marquette University, michael.ryan@marquette.edu

Influence of RTIL Nanodomains on the Voltammetry and Spectroelectrochemistry Of Fullerene C_{60} in Benzonitrile/Room Temperature Ionic Liquids Mixtures

Abderrahman Atifi
Chemistry Department, Marquette University
Milwaukee, Wisconsin

Michael D. Ryan
Chemistry Department, Marquette University
Milwaukee, Wisconsin

Abstract: The cyclic voltammetry of fullerene C_{60} was examined in mixed benzonitrile/RTIL solvents in order to probe the effect of nanodomains in the mixed RTIL/benzonitrile solutions and their effect upon the voltammetry. In probing the interactions of the fullerides (up to C_{60}^{3-}) with RTILs, $BMIm^+$ (1-butyl-3-methylimidazolium, mostly planar) and tetraalkylammonium (more spherical/flexible) salts were used. In order to investigate these shifts in more detail, the $\Delta E_{12}°$ ($=E°_1-E°_2$) and $\Delta E_{23}°$ ($=E°_2-E°_3$) values, which were independent of the reference potential, were used. At higher concentrations of the RTILs, greater stabilization of the more highly charged fullerides were observed. These shifts were attributed to the interaction of the fullerides with nanodomains of the RTIL. This was further confirmed by examining the shifts in the $E_{1/2}$ values of non-RTIL and RTIL salts at constant ionic strength and the changes in diffusion coefficient with %RTIL. The observed shifts in the $E_{1/2}$ values with increased concentration of the RTIL salts could not be

[Electrochimica Acta, Vol 191, (February, 2016): pg. 567-576. DOI. This article is © Elsevier and permission has been granted for this version to appear in e-Publications@Marquette. Elsevier does not grant permission for this article to be further copied/distributed or hosted elsewhere without the express permission from Elsevier.]

explained by ion pairing equilibria alone. Changes in the visible and near infrared spectra between benzonitrile and mixed benzonitrile/RTIL spectra were most significant for C_{60}^{3-}, where voltammetric evidence indicates the strongest interaction between the fullerides and the RTIL. Among the RTILs studied, preliminary DFT calculations showed that the more flexible tetraalkylammonium ion was able to stabilize the C_{60}-anionic species better than the planar $BMIm^{+}$ species, under similar solution conditions.

Graphical abstract

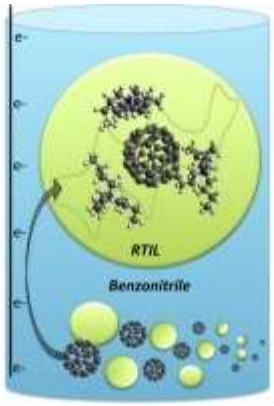

Keywords: RTIL, C60, spectroelectrochemistry, cyclic voltammetry

1. Introduction

Ionic liquids are generally formed by the combination of a large organic cation and a small anion. Due to these size constraints, the coulombic attractions are weakened, preventing the formation of solids at room temperature. Room temperature ionic liquids (RTILs) possess short-range organization due to electroneutrality, but lack long-range structures that would lead to solid crystals. As a result, RTILs can be considered as structured, nano-segregated liquids. The structure of an RTIL in the presence of molecular solvents has been examined using molecular dynamics. Mixtures of RTILs with molecular solvents lead to four recognized regimes, depending upon the ratio of RTIL/molecular solvent. At low concentrations of the RTIL, they behave as an electrolyte in solution. As the concentration of the RTIL increases, aggregates (nanodomains) form. In RTIL-rich mixtures, the molecular solvents will become a dilute solute, interacting with the RTIL domains, breaking up the ionic network. The fourth regime is the neat RTIL. Unlike surfactants, molecular dynamics shows that the RTIL

nanodomains in RTIL/molecular solvent mixtures have a filamentous structure along with isolated ions in the aggregate regime. The formation of these aggregates can occur at relatively low mole fractions of the RTIL (e.g., 0.06 in the simulation involving acetonitrile).

Previously, in this laboratory, the electrochemistry of 1,4-dinitrobenzene (DNB) was studied using mixed molecular/room temperature ionic liquid (RTIL) solutions. This work indicated that nanostructures of molecular and RTIL domains were present in the mixed solvents systems. In this case, the planar geometry of DNB^{2-} favored inclusion in the RTIL domains. Direct spectroscopic evidence was later obtained for nanodomains in the electrochemistry of nickel porphinone in THF/RTIL mixtures. In order to investigate the effect of molecular structure on the voltammetric behavior of solutes in mixed molecular solvent/RTIL solutions, the electrochemistry of C_{60} was studied. Unlike DNB, C_{60} and its redox products are spherical and the charge is diffusely distributed. To investigate this, two types of RTILs were used in this work. The first type contained the planar $BMIm^+$ cation, which contains an ionic environment where ion pairing with the spherical redox species is poor. The second type contained a tetraalkylammonium cation, where the flexibility of the cation provided for better ionic interaction.

Buckminsterfullerene, C_{60}, can be reduced in aprotic solvents in six one-electron waves. Five reversible waves were observed by Dubois et al using cyclic voltammetry. A reversible sixth wave was observed at low temperatures by Xie et al. and by Ohsawa and Saji. The products of the first three waves can be generated by coulometry or spectroelectrochemistry or isolated as salts by chemical reduction. The spectroelectrochemical reduction of C_{60} caused the bands at 257 and 330 nm to shift to 262 and 339 nm, respectively, with a decrease in absorbance. Further reduction to C_{60}^{2-} led also to a small red, shifts in the λ_{max} values (263, 340 nm). Changes in the near infrared spectrum though were much more informative of the oxidation state of the fulleride. The near infrared spectrum of C_{60}^- had a strong band at 1073 nm, with weaker bands at shorter wavelengths (995, 917 nm). The major band has been assigned to the allowed $t_{1u} \rightarrow t_{1g}$ transition, and the weaker bands to vibrational fine structure. The dianion of

C_{60}has bands at 952 and 830 nm and the trianion at 1367, 956, 878 and 788 nm.

The effect of supporting electrolyte and solvent properties on the redox potentials was studied by Dubois et al. and Noviandri et al. The latter study examined the shifts based on the Kamlet/Abboud/Taft and Fawcett models. They emphasized the importance of using decamethyl ferrocenium as the reference potentials in order to minimize the effect of solvent on the reference potential. Using this reference system, a positive slope of $E_{1/2}$as a function of the Gutmann acceptor number (AN) was observed for all the waves studied as expected due to the stabilization of the anionic species by the Lewis acidity of the solvent. The relative importance of the solvent acidity/basicity, solvent dipolarity and polarizability (for the Kamlet/Abboud/Taft model) or the polarity/polarizability and the Gutmann AN/DN (donor number) (Fawcett model) was calculated.

Jehoulet et al. studied the redox behavior of C_{60} in redox films with acetonitrile as solvent. Four reduction waves were observed in the films. Adamiak and Opalla studied C_{60} in cast 1,2-dichlorobenzene films in contact with aqueous solutions. Association between the anionic C_{60} species and the tetraalkyl ammonium cations were observed. Limited studies have been carried out in RTILs because of the insolubility of C_{60} in those solvents. Duffy and Bond have studied the voltammetry of C_{60} in toluene using a phosphonium-phosphate ionic liquid as an electrolyte. The electrochemistry of C_{60} films in contact with N-butyl-N-methylpyrrolidium-based ionic liquids was studied by Ueda et al. In this case, six waves were observed using cyclic voltammetry. Damlin et al. used FTIR to study cast C_{60} films in contact with three different RTILs. Under the conditions studied, the film was stable over the first three reductions when $BMImPF_6$, $BMImBF_4$ and $DBiMImBF_4$ (BMIm: 1-butyl-3-methylimidazolium; DBiMIm: 1-butyl-2,3-dimethylimidazolium) was the solvent. These results indicated that the four redox species (C_{60}, C_{60}^{-}, C_{60}^{2-}, C_{60}^{3-}) had limited solubility under these conditions, though some dissolution was observed. On the other hand, the slow diffusion of redox species in RTILs may have masked the amount of dissolution.

As discussed above, mixed molecular/RTIL solution are not homogeneous, creating RTIL and molecular solvent domains within the solution (nanodomains). The formation of these RTIL domains may lead to more efficient catalysis because the RTIL domains may stabilize charged species while the molecular domain may solubilize the other reagent(s). An example of efficient catalysis in mixed solvents is the reduction of CO_2 to CO in mixed $EMImBF_4$/water solutions. The stabilization of CO_2^- in mixed DMF/RTIL solutions has been examined both experimentally and by DFT calculations for the electroreduction of CO_2in DMF solutions with low concentrations of RTIL. Shi et al. used mixed RTIL/propylene carbonate solutions for the electrochemical reduction of CO_2 to CO. Mixed RTIL/acetonitrile solutions were used by Sun et al. to switch the reaction course for the electrochemical reduction of CO_2. Because RTILs can be tailored for specific tasks, such as metal coordination or CO_2 capture. significant functionality can be added to the RTIL. Mixed solvents may overcome the problems of the high cost of RTILs and unfavorable physical properties (e.g., high viscosity) while maintaining the reactivity in the RTIL. These studies confirm the importance of mixed RTIL/molecular solvents in electrocatalytic systems.

2. Experimental

2.1. Chemicals

High purity RTILs 1-butyl-3-methylimidazolium hexafluorophosphate ($BMImPF_6$), and 1-butyl-3-methylimidazolium tetrafluoroborate ($BMImBF_4$) were purchased from Merck and were employed without further purification, except as noted in the text. Ethyldimethylpropylammonium bis(trifluoromethylsulfonyl) imide ($AmNTf_2$), 1-butyl-3-methylimidazolium chloride (BMImCl), anhydrous benzonitrile, triethylphosphine oxide ($POEt_3$), diphenylphosphorus oxychloride (Ph_2POCl) and decamethylferrocene were purchased from Sigma–Aldrich Chemical Co. and were used as received. Tetrabutylammonium perchlorate (TBAP, GFS Chemical Co.) was used as electrolyte in molecular solvent experiments.

2.2. Procedures

All solutions (voltammetric and spectroelectrochemical) were prepared in a glovebox under an argon atmosphere. The cells were sealed if measurements had to be made outside the glove box. Voltammetric data were obtained in the glove box. Using this procedure, the solutions were never exposed to dioxygen or water. A homemade small volume cell was used for controlled potential electrolysis of C_{60} in the pure RTIL. A gold mesh was used as a working electrode, silver wire as pseudo-reference and platinum wire as auxiliary electrode. The two compartments were separated by glass frit. While stirring the solution during the electrolysis, electrogeneration of reduced species was obtained by setting the potential at the corresponding wave.

2.3. Instrumentation

Cyclic voltammetry was carried out at a platinum electrode (1.6 mm or 10 μ) using a Model 600D Series Electrochemical Analyzer/Workstation (CHI Version 12.06). A low-volume thin layer quartz cell which was purchased from BAS Instruments was used for UV-visible spectroelectrochemical experiments. A platinum mesh was used as working electrode and a silver wire was used as auxiliary electrode. Potentials were measured relative to Ag/0.1 M $AgNO_3$. UV/visible spectra were recorded on a HP8452A diode array spectrophotometer. For UV-visible experiments, the entrance window of the cell was masked so that the spectral beam passed only through the working electrode. Near infrared spectra were recorded using Cary Series UV–Vis–NIR spectrophotometer (Agilent Technologies). ^{31}P-NMR measurements were performed using a Varian 400 MHz FT spectrometer. The viscosity of the solutions were measured using a Brookfield DV2T viscometer, and the temperature was controlled with a water bath.

2.4. Computational methods

The Gutmann acceptor numbers were calculated using the NMR procedure of Schmeisser et al. This procedure was developed to determine AN in RTILs. The ^{31}P chemical shift of Et_3PO was measured

at a series of concentrations and extrapolated to infinite dilution. From the chemical shift, the acceptor number was calculated using an empirical equation. The variation in the Gutmann AN was nonlinear with respect to volume %RTIL. Typical data for $AmNTf_2$ are shown in the Supplementary Information (Figure S1). Non-linear behavior between %RTIL in molecular solvent mixtures and the polarity parameter π* has already been reported. Evolving factor analysis of the visible spectroelectrochemical data was carried out using MATLAB. Computational calculations were performed at the density functional theory (DFT) level as implemented in the Gaussian 09 program. Optimized geometries of ion pairs and clusters of ions were computed using m06 method and the 6–31 G basis set. Implicit solvation in acetonitrile was included by polarizable continuum model (PCM). All calculations converged to minima, and all frequencies were positive numbers. The ΔE redox potentials between the first three reductions were calculated from the disproportionation energies, zero point energy corrected ($\Delta E = \Delta G_{disp}/F$).

3. Results and Discussion

3.1. Cyclic voltammetry

The cyclic voltammetry of C_{60} was examined in a series of benzonitrile/RTIL mixtures. The starting material, C_{60}, was not soluble in pure ionic liquids, but had significant solubility in solutions up to 60% (v/v) RTIL/benzonitrile, making it possible to measure the $E_{1/2}$ values in the mixed solvents. The first three waves of C_{60} were reversible in RTIL mixtures as shown in Fig. 1 for benzonitrile and 20% benzonitrile/$AmNTf_2$ solutions. As can be seen in the figure, the first wave did not shift significantly with the presence of the RTIL, while the second and third waves exhibited larger shifts. The cyclic voltammogram of C_{60}^- in $AmNTf_2$was obtained after the electrolysis of C_{60}, as described in the Experimental Section (Fig. 2). Reversible waves were observed for the C_{60}^-/C_{60}^{2-} and C_{60}^{2-}/C_{60}^{3-} couples in $AmNTf_2$. The C_{60}/C_{60}^- wave was not reversible in $AmNTf_2$, probably due to the insolubility of C_{60}itself. The shift in $E_{1/2}$ values (vs decamethylferrocene) for the first three waves were obtained for mixtures of benzonitrile with $BMImPF_6$, $BMImBF_4$ or $AmNTf_2$ (Supplementary Information, Table S1, Figure S2). For all

these solvent mixtures, the first three waves of C_{60}shifted to more positive potentials as the %RTIL increased. As expected, the redox potential of the third wave was most sensitive to the %RTIL; the first wave was the least sensitive. The potential shifts depended upon both the %RTIL and the identity of RTIL. For a given %RTIL, larger shifts were observed for the $BMIm^+$ RTILs as compared to $AmNNTf_2$mixtures.

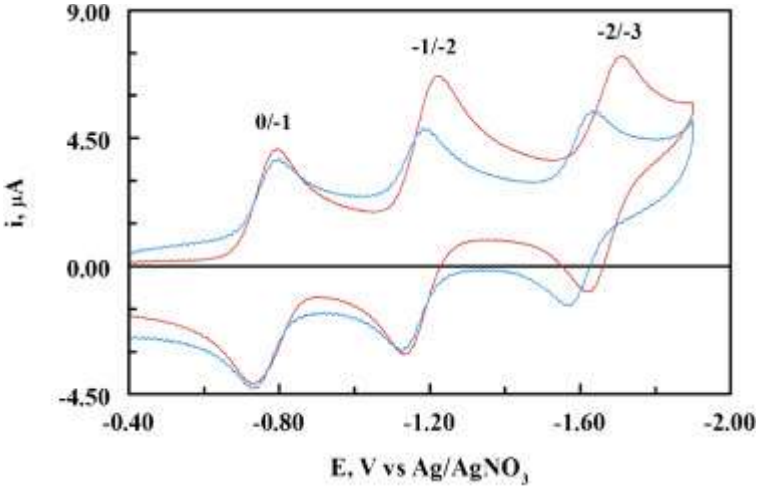

Fig. 1. Cyclic voltammetry of 0.48 mM C_{60} in benzonitrile/0.10 M TBAP (red) and 0.40 mM C_{60} in 20% $AmNTf_2$ (blue). Scan rate: 1.0 V/s. (For interpretation of the references to color in this figure legend, the reader is referred to the web version of this article.)

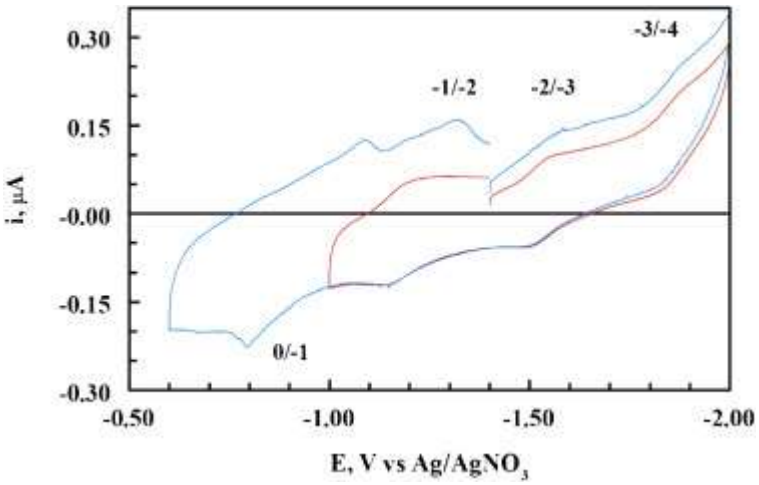

Fig. 2. Cyclic voltammetry of C_{60}^{2-} in $AmNTf_2$. Red line: positive scan switched at −1.0 V; Blue line: positive scan switched at −0.60 V.

The variation in the $E_{1/2}$ values for the first three waves as a function of the Gutmann AN is shown in Fig. 3. The method of Schmeisser et

al. as described in the Experimental section, was used to measure the Gutmann AN of benzonitrile/RTIL mixtures. Good linear relationships between the $E°_{1/2}$ values and AN were observed for benzonitrile/RTIL mixtures for all three waves (Fig. 3), with the potentials referenced versus decamethylferrocene. This is in contrast for molecular solvents where the Gutmann acceptor numbers did not correlate well with the $E_{1/2}$ values (black symbols in Fig. 3). A better correlation could be expected here because the solvent (benzonitrile) remains the major solvent species, on a molar basis, in all the solutions. As a result, the solvation environment remains similar, at least for low to moderate concentrations of the RTIL. Some important differences are seen though for the third wave. For the first two waves, there is no significant difference in the $E_{1/2}$waves of the three RTILs, when plotted versus the Gutmann AN. For the third wave (Fig. 3C), though, the $E_{1/2,3}$ values of $AmNTf_2$ solutions for a given Gutmann AN are consistently positive of the values obtained with the $BMIm^+$ RTILs, and the data were less linear. This is in contrast to Fig. S2 where larger $E_{1/2}$ shifts were observed for $BMIm^+$ RTILs when the data were plotted as a function of %RTIL. This difference is due to the higher Gutmann AN for $BMIm^+$ salts.

[Electrochimica Acta, Vol 191, (February, 2016): pg. 567-576. DOI. This article is © Elsevier and permission has been granted for this version to appear in e-Publications@Marquette. Elsevier does not grant permission for this article to be further copied/distributed or hosted elsewhere without the express permission from Elsevier.]

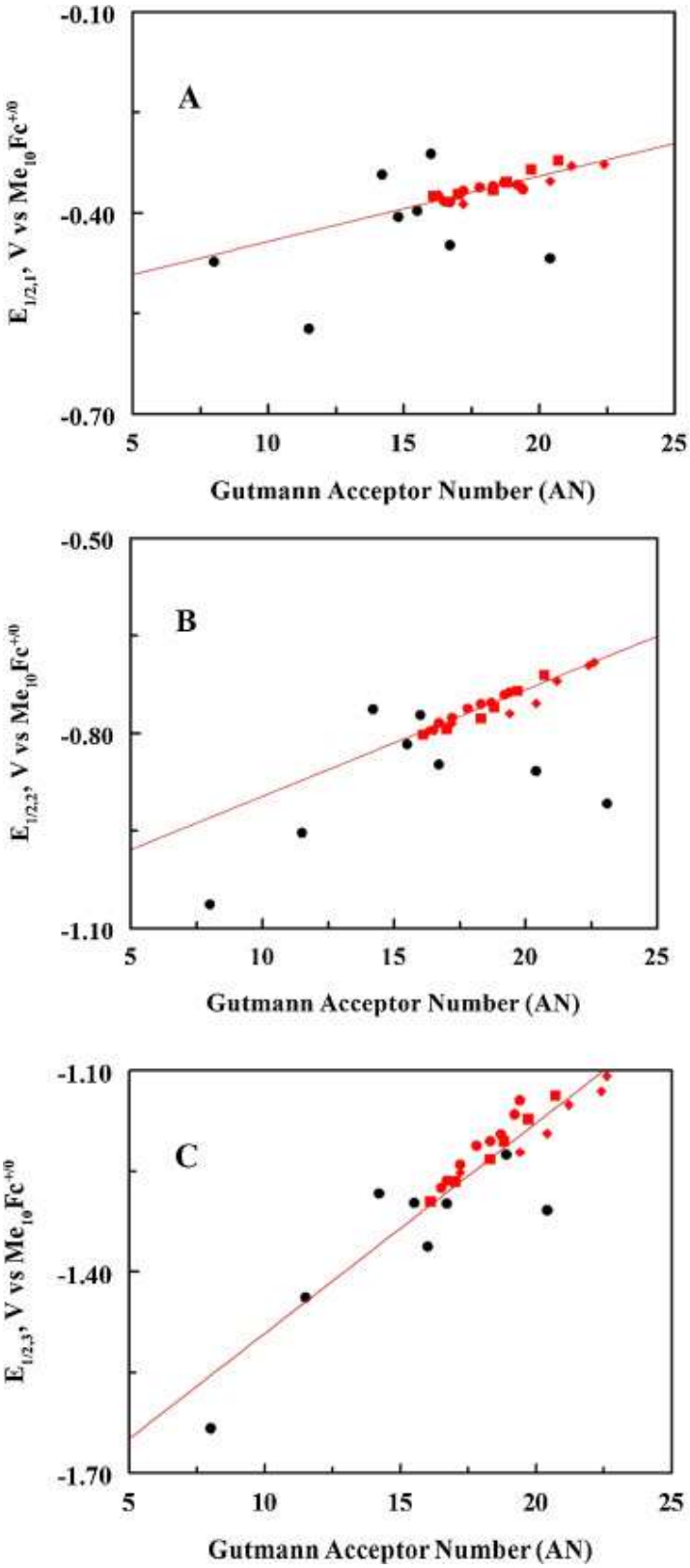

Fig. 3. Variation in the $E°_{1/2,1}$ (A), $E°_{1/2,2}$ (B) and $E°_{1/2,3}$ (C) values for C_{60} in mixtures of benzonitrile and RTILs. Black symbols are molecular solvents. Red symbols are for benzonitrile/RTIL mixtures: $AmNTf_2$ (circles), $BMImPF_6$ (diamonds), $BMImBF_4$ (squares). Least square fit slopes for benzonitrile/RTIL mixtures only: first wave: 1.0×10^{-2}, ($R^2 = 0.90$) second wave: 1.6×10^{-2}, ($R^2 = 0.95$), third wave: 2.6×10^{-2} ($R^2 = 0.93$).

While the data in Fig. 3 have the advantage that the potentials were referenced versus the decamethylferrocene couple, the results are still dependent upon the choice of reference system. The use of potential differences between the C_{60} redox potentials ($\Delta E°_{12} = E°_1 - E°_2$; $\Delta E°_{23} = E°_2 - E°_3$) removes the need for reference potentials and the ambiguities that it creates. The differences in the $E_{1/2}$ values between the first and second waves ($\Delta E°_{12}$) along with the trend line are plotted in Fig. 4A. For lower concentrations of the RTIL, the $\Delta E°_{12}$ values are well correlated with Gutmann AN. The slope was found to be −0.0064 V. At higher concentrations, the $\Delta E°_{12}$ values deviated from the trendline for molecular solvents and low concentrations of the RTIL. This indicates that there was additional stabilization of the reduced species, beyond what would be expected from the Gutmann AN. Similar results were observed for $\Delta E_{23}°$ (Fig. 4B).

[Electrochimica Acta, Vol 191, (February, 2016): pg. 567-576. DOI.

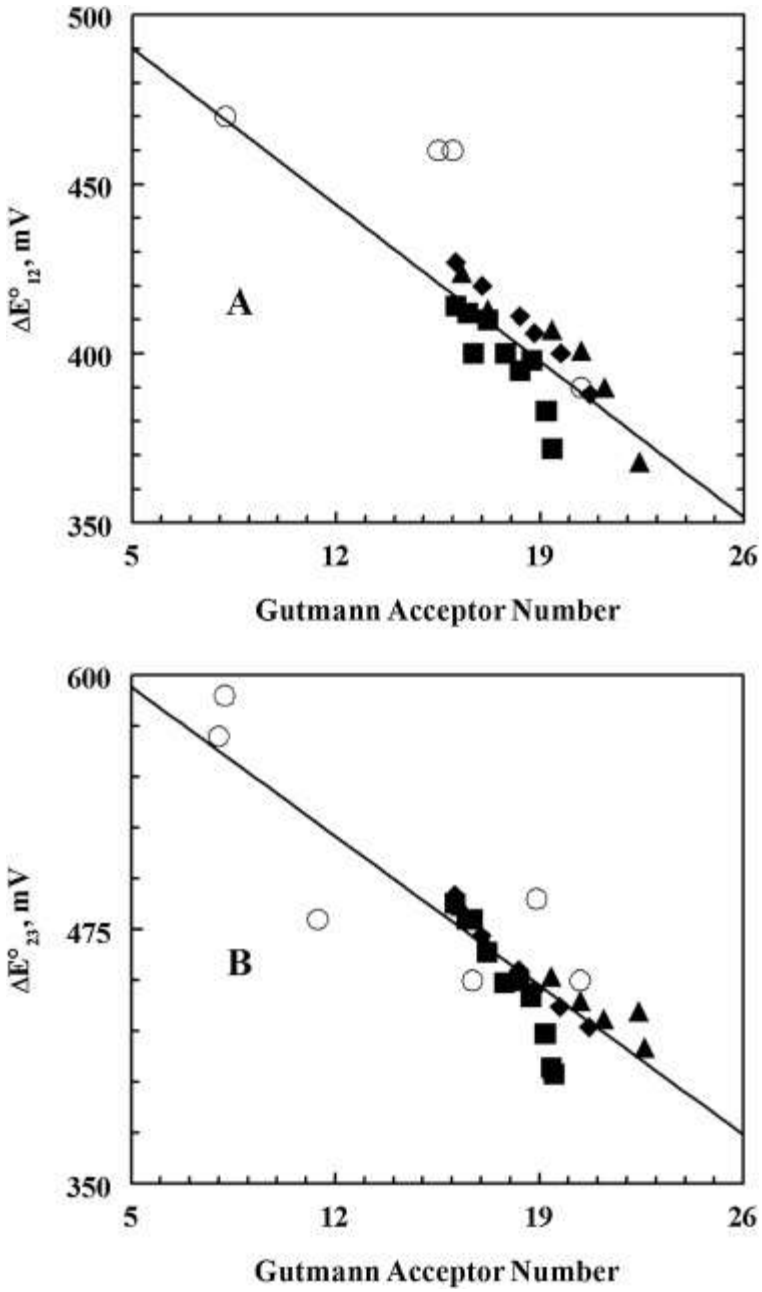

Fig. 4. Variation in $\Delta E_{12}°$ (A) and $\Delta E_{23}°$ (B) values as a function of the Gutmann AN. Data from Dubois et al. (○); benzonitrile/$AmNTf_2$ mixtures (■); benzonitrile/$BMImPF_6$ (▲); benzonitrile/$BMImBF_4$ (♦). The trendlines are based on the data.

In order to sort out the effects due to ion pairing and the presence of RTIL domains, the cyclic voltammetry of C_{60} in salts that do not form RTILs was carried out, and compared with the results for RTIL salts. In order to maintain the ionic strength constant, the total

concentration of TBAP and the added salt was kept constant at 0.50 M. For the first wave, two ion pairing equilibria can occur for mixtures of TBAP/BMImCl:

$$(C_{60}^{-}) \quad K_{IP1,TBA^{+}C_{60}^{-}}$$

$$(C_{60}^{-}) \quad K_{IP1,BMIm^{+}C_{60}^{-}}$$

Similar reactions can be written for C_{60}^{2-}, and C_{60}^{3-}, with the subscript after IP indicating the number of cations ion paired with the C_{60}-anionic species. The detailed analysis for the first three waves of C_{60} for mixtures of TBAP/BMImCl is shown in the Supplementary Data (Figures S3-S5). The results are summarized in Table 1. A similar approach was used for the analysis of other salt mixtures (Table 1). The $E_{1/2}$ values as a function of the salt concentration for the first three waves of C_{60} are shown in Fig. 5, along with the theoretical lines based on the constants in Table 1.

Table 1. Ion Pairing Equilibrium Constants for Fulleride Species.

C_{60}-Species	**Salt**	**K_{IP1}**	**K_{IP2}**	**K_{IP3}**
C_{60}^{-}	TBAP	1.5 ± 0.3	–	–
	THAP	5 ± 1	–	–
C_{60}^{2-}	TBAP	13 ± 4	2.4 ± 0.7	–
	THAP	35	1.3	–
	$AmNTf_2$	3	–	–
	$BMImPF_6$	2	–	–
C_{60}^{3-}	TBAP	36	20	0.5
	THAP	60	5	–
	$AmNTf_2$	650		
	$BMImBF_4$	500	–	–
	$BMImPF_6$	800	–	–

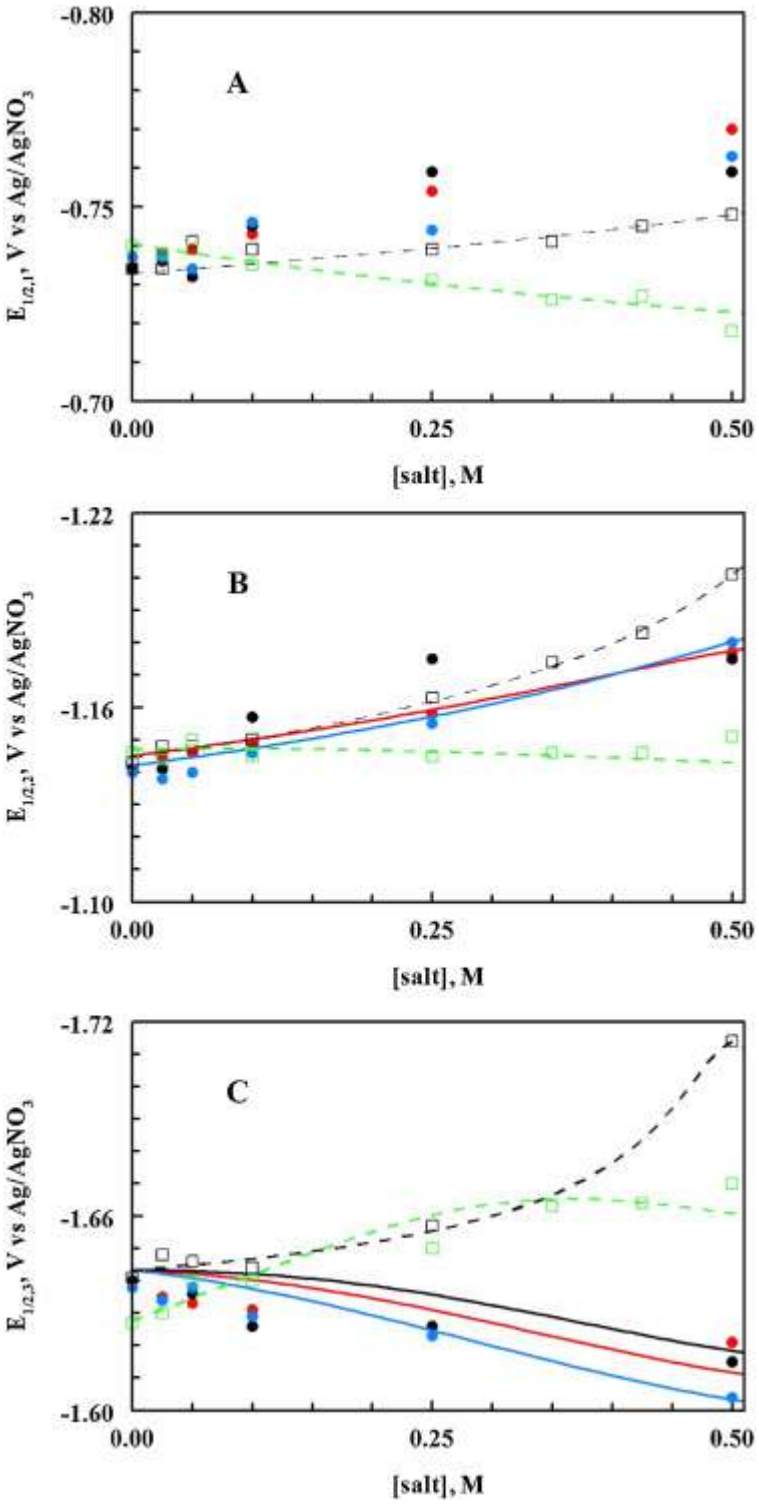

Fig. 5. $E_{1/2,1}$ (A), $E_{1/2,2}$ (B) and $E_{1/2,3}$ (C) as a function of the salt concentration. Salts: BMImCl (□, black dashed line), THAP (□, green dashed line), $AmNTf_2$ (●, red solid line), $BMImBF_4$ (●, black solid line), $BMImPF_6$ (●, blue solid line). C_{TBAP} + C_{salt} = 0.50 M. Theoretical lines correspond to the predicted shifts in $E_{1/2}$ values based on K_{IP} values

in Table 1. Solvent: benzonitrile. (For interpretation of the references to color in this figure legend, the reader is referred to the web version of this article.)

The shift in the $E_{1/2,1}$ values as a function of the salt concentration are shown in Fig. 5A. The negative shift in the $E_{1/2,1}$ values as the concentration of BMImCl increased indicated that TBA^+ ion paired more strongly with C_{60}^- than $BMIm^+$. There was no evidence for ion pairing between $BMIm^+$ and C_{60}^-. On the other hand, THA^+ ion paired slightly stronger with C_{60}^- than TBA^+, probably due to the longer more flexible alkyl chains. The observed shifts were consistent with the previous work by Dubois et al. The $E_{1/2,1}$ values for the RTIL salts shifted to more negative potentials indicating that there was little interaction between these salts and C_{60}^-. This is understandable for the $BMIm^+$ salts, as $BMIm^+$ does not ion pair with C_{60}^-, but is unexpected for the Am^+ salt as Am^+ should ion pair with C_{60}^- about as strongly as TBA^+. In fact, the $E_{1/2,1}$ values for the RTIL salts are negative of the values observed for BMImCl. These results indicate that solvation factors other than ion pairing are controlling the $E_{1/2,1}$ values. These shifts were relatively small, and would be difficult to quantitate.

The shifts for $E_{1/2,2}$ were generally consistent with ion pairing, with smaller shifts observed for the RTIL salts compared to BMImCl/TBAP mixtures (Fig. 5B). For THAP/TBAP mixtures, small shifts in the $E_{1/2,2}$ value was observed consistent with similar K_{IP} values for TBA^+ and THA^+. The observed shifts for $E_{1/2,2}$ for the RTIL salts were consistent with a small K_{IP1}between the salt and C_{60}^{2-}, and no measurable value for K_{IP2} (though one was observed for TBAP and THAP). The largest differences was seen for the third wave (Fig. 5C). The replacement of TBA^+ ion with $BMIm^+$ (as BMImCl) shifted the potentials more negatively due to the weaker ion pairing with $BMIm^+$. On the other hand, the $E_{1/2,3}$ shifted positively for the three RTIL salts, indicating a strong interaction of the salt with C_{60}^{3-}, even though $BMIm^+$and Am^+ do not ion pair with C_{60}^{3-} stronger than TBA^+. In addition, while a large K_{IP1} was observed for the ion pairing of the RTIL salts with C_{60}^{3-}, no measurable value was seen for K_{IP2}. This indicates that the RTIL salts interact with C_{60}^{3-} as a unit (nanodomains) rather than individual free cations (like TBA^+ in TBAP). Weaker, but similar, behavior was observed for the RTIL salts and the second wave of C_{60}. Overall, the interaction of the RTILs with the fulleride anions cannot be

predicted based on successive ion-pair equilibria, as were observed for other salts. The stabilization was stronger than predicted by ion pairing and the RTIL nanodomains appeared to interact as a single unit.

The differences in ion pairing with tetraalkylammonium ions is most noticeable between tetramethylammonium (TMA^+) and the dianion of dinitrobenzene (DNB^{2-}) in acetonitrile (K = 195), which decreased to 3 for TEA^+. The TBA^+ and tetraoctylammonium formation constant with DNB^{2-} were identical. Recent theoretical work by Fry has shown that the highest positive charge on the tetraalkyl ammonium ion was on the α-methylene of the tetraalkylammonium chain. Ion pair formation is almost completely due to the electrostatic attraction between α-protons and the anion. The spherical nature of the C_{60}-species may make it easier to the α-protons to interact with the anions without steric problems because of the curvature of the anion (unlike DNB^{2-}, which is planar). This can be seen in Figure S6, where two of the α-methylene protons can interact well with the fulleride. For larger cations though, it may be difficult for three cations to ion pair with C_{60}^{3-} because of the longer alkyl chains, causing a fall off of the K values for the 2nd and 3rd ion pair with C_{60}^{3-}.

Fig. 6 shows that variation in the $\Delta E_{23}°$ values as a function of the concentration of added salt. The addition of BMImCl has little effect on the $\Delta E_{12}°$ (not shown) and on the $\Delta E_{23}°$ values. The lines in Fig. 6 are based on the predicted $\Delta E_{23}°$ values, using the equilibrium constants in Table 1. On the other hand, addition of $BMIm^+$ as the BF_4^- or PF_6^- salt caused a measurable decrease in the $\Delta E_{23}°$ values (similar results but with smaller changes were observed for $\Delta E_{12}°$ values), even though $BMIm^+$ ion pairs more weakly with the C_{60}-anionic species than TBA^+. The final feature that is significantly different between the non-RTIL and RTIL salts is the relationship between the shift in potential and concentration. For the non-RTIL salts, the shifts are as expected with successive ion pairing constants (K_{IP1}, K_{IP2}, K_{IP3}), leading to first, second and third power relationships between the salt concentration and the $E_{1/2}$. For the RTIL salts ($BMImBF_4$, $BMImPF_6$ and $AmNTf_2$), the potential shifts can be explained by one K_{IP} value and a first order concentration relationship between the half wave potential and the RTIL concentration. It is unlikely that a single $BMIm^+$ cation would displace 2–3 TBA^+ cations,

given that $BMIm^+$ forms weaker ion pairs. The more likely explanation is that fullerides are extracted into RTIL domains, where they are solvated by 2–3 cations of the RTIL. It is not clear at this time whether the anions template the RTIL nanodomains or whether the nanodomains are formed prior to the interaction with the C_{60}anion.

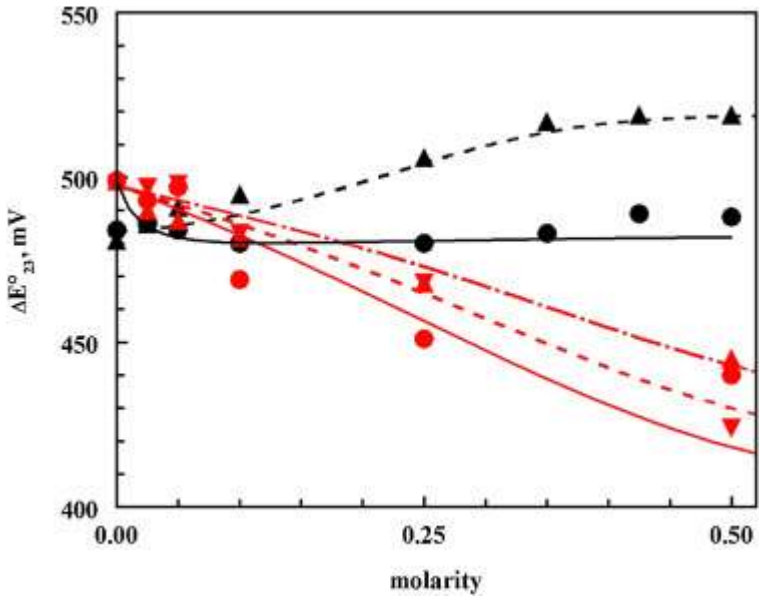

Fig. 6. Dependence of the $\Delta E°_{23}$ values in the concentration of the electrolyte concentration. Electrolyte: BMImCl (●), THAP (▲), $BMImBF_4$ (●), $BMImPF_6$ (▼), $AmNTf_2$ (▲). Solid line is for ion pairing between TBA^+ and anionic C_{60} species: $K_{IP1,C60-} = 15$, $K_{IP1,C60(2-)} = 80$, $K_{IP2,C60(2-)} = 80$, where K_{IP1} and $K_{IP2}$are for the ion pairing of the first and second TBA^+ cation with the anion. For all the electrolytes: $M_{addedsalt} + M_{TBAP} = 0.50$ M. Solvent: benzonitrile.

Preliminary work has begun using DFT calculations to understand the solvation of the C_{60}anions with $BMIm^+$ and Am^+ cation (for simplicity, TBA^+ was used instead of the ethyldimethylpropylammonium cation). From the disproportionation reactions, the ΔG_{disp} can be calculated:

(1) $2\ Cat^+C_{60}^- \rightarrow C_{60} + (Cat^+)_2C_{60}^{2-}$

(2) $2\ (Cat)_2C_{60}^{2-} \rightarrow (Cat^+)C_{60}^- + (Cat^+)_3C_{60}^{3-}$

where Cat^+ is the cation of the RTIL (see Supplementary Information Figure S6 for $(TBA)_3C_{60}$ and $(BMIm)_3C_{60}$ structures). Using this value, the ΔE_{12} and ΔE_{23} values can be theoretically calculated.

The changes in the ΔE_{12} and ΔE_{23} values without ion pairing (but solvated) to the values with ion pairing is shown in Table 2. Ion pairing of reduced species with Na^+ cations results in stabilization of ΔE_{12} and ΔE_{23} by 268 and 203 mV, respectively. Interestingly, a larger stabilization was observed for $BMIm^+$ (238 and 228 mV) and TBA^+(359 and 267 mV) cations, as one would expect less interaction of reduced species with big cations compared to the small acidic Na^+ cation. Such stronger interactions could be due to significant hydrogen bonding contribution. Hydrogen bonding of reduced species with imidazolium cation is reported in literature. In the case of the dianion and trianion, particularly, such hydrogen-bonding network may be a template of clusters formation of cations around the reduced species. In comparing the differences between ion pairing by $BMIm^+$ with Am^+, the tetraalkylammonium ion is able to reduce the ΔE_{12} value by 121 mV and the ΔE_{23} value by 39 mV. Comparing the experimental ΔE_{12} and ΔE_{23} with the same acceptor numbers, we obtain differences of 30 and 48 mV, respectively. The predicted stabilization overestimated the ΔE_{12} value, while the ΔE_{23} value is reasonably close to the predicted value. The better correspondence with the ΔE_{23} as compared to the ΔE_{12} values is probably due to the stronger ion pairing with the more negatively charged species. In both cases, better stabilization was observed for the more flexible tetraalkylammonium ion with the spherical C_{60} species, than with the planar $BMIm^+$ cation. More detailed calculations are needed to account for the presence of the anion in the cluster in order to calculate the more realistic nanodomains that are present in the RTIL solutions. The absence of the counter anions is probably the source of the underestimation of the ΔE values, as compared to the experimental values.

Table 2. Effect of Ion Pairing on the DFT Calculations for Disproportionation Reactions (Reactions 1–2).

	No ion paring		**Na^+**		**$BMIm^+$**		**TBA^+**	
	First	**Second**	**First**	**Second**	**First**	**Second**	**First**	**Second**
Δ*G* (kJ/mol)	65.21	44.45	39.39	24.86	42.25	22.50	30.61	18.73
Δ*E* (V)	0.676	0.461	0.408	0.258	0.438	0.233	0.317	0.194

In addition to a shift in the redox potential, the diffusion current decreased as the %RTIL increased. Qualitatively, this is consistent with the increase in the viscosity of the benzonitrile/RTIL mixtures.

The variation in the diffusion coefficients of electroactive materials generally follow the Stokes-Einstein equation.

$$(3)\quad D = \frac{k_B T}{6\pi\eta r}$$

where k_B is the Boltzmann constant, T is the temperature, η is the viscosity, and r is the hydrodynamic radius of the diffusing species. The diffusion of electroactive materials in RTILs and molecular solvents has been observed to follow the Stokes-Einstein relationship. A modified version of the Stokes-Einstein equation was used by Vorotyntsev et al. to account for the high viscosity of RTILs. In both cases, the functional relationship between D and η is the same. The Stokes-Einstein equation works reasonably well even for large changes in viscosity, as has been seen for ferrocene in acetonitrile (0.34 cP) and $BMImPF_6$ (308 cP). In order to determine if the diffusion currents in molecular solvent/RTIL mixtures quantitatively follow the Stokes-Einstein equation, the diffusion coefficient ratios were calculated based on the peak current for the first wave in benzonitrile and benzonitrile/RTIL mixtures. The current in cyclic voltammetry at a macroelectrode is proportional to the square root of the diffusion coefficient:

$$(4)\quad i_{p,BzCN} = \text{constant} \times D_{BzCN}^{1/2} = \text{constant}/\eta_{BzCN}^{1/2}$$

$$(5)\quad i_{p,mixture} = \text{constant} \times D_{mixture}^{1/2} = \text{constant}/\eta_{mixture}^{1/2}$$

Therefore,

$$(6)\quad \frac{D_{mixture}}{D_{BzCN}} = \left(\frac{i_{p,mixture}}{i_{p,BzCN}}\right)^2 = \frac{\eta_{BzCN}}{\eta_{mixture}}$$

Fig. 7 shows that the viscosity ratio of the solution ($\eta_{BzCN}/\eta_{mixture}$, red line) decreased in an exponential manner as a function of the%$AmNTf_2$ as expected for molecular solvent/RTIL mixtures. The ratio of diffusion coefficients ($D_{mixture}/D_{BzCN}$, green circles) were also plotted in Fig. 7. If Eq. (6) (from Stokes-Einstein equation) was

observed for mixtures, the diffusion coefficient ratios should follow the same line as the viscosity ratios. Experimentally, the diffusion coefficient ratios of C_{60} decreased much more modestly, especially for %RTIL less than 20%. This indicates that the diffusion coefficient is not inversely proportional to the measured viscosity.

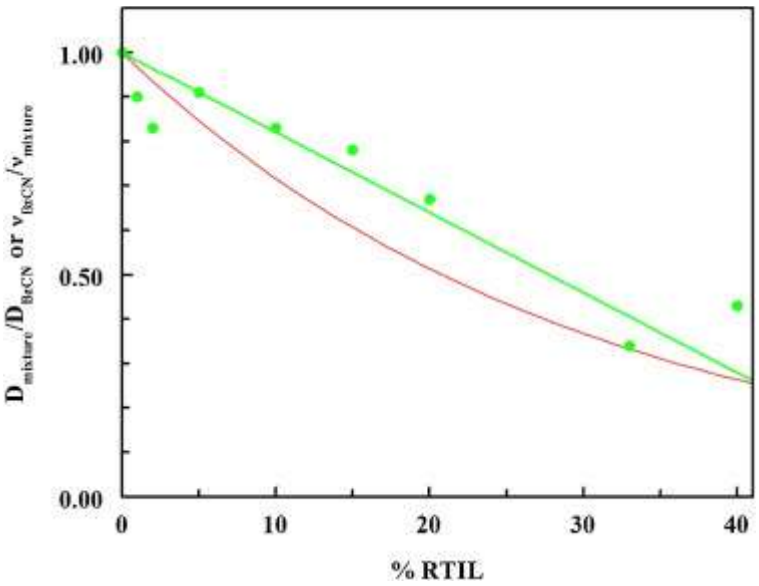

Fig. 7. Variation of viscosity of the solution at a function of%$AmNTf_2$ (red line), normalized to the viscosity of benzonitrile at 25 °C. The green filled circles are the ratio of the diffusion coefficients between the RTIL mixtures and pure benzonitrile based on the first peak current. The green line is the best fit to the ratio of $D_{mixture}/D_{BzCN}$. (For interpretation of the references to color in this figure legend, the reader is referred to the web version of this article.)

Previous work has shown that the supermolecular structure of the pure RTIL state is maintained in mixture solvents. As a result, there will be molecular solvent and RTIL domains in the mixed solvents, especially as the %RTIL increases. The electroactive material, C_{60}, is insoluble in the RTILs studied, and one would expect them to be insoluble in the RTIL domains of the mixed solvent (though the reduced materials may indeed be soluble in the RTIL domains). Therefore, one would expect that C_{60} would diffuse almost exclusively through the molecular solvent domains which will probably have a microviscosity less than the measured viscosity. The best fit line for the observed ratio of the diffusion coefficients is shown as the green line in Fig. 7. This indicates a linear relationship between the diffusion coefficient and the %benzonitrile in the mixture. This would be

consistent with the obstruction of the diffusion of C_{60} (which is insoluble in the RTIL) by the RTIL nanodomains. This relationship reasonably predicts the diffusion coefficient ratios for the RTIL/benzonitrile mixtures better than the viscosity up to the point where C_{60} ceases to be soluble in the mixtures. While there are only a few points for the low concentration of the RTIL, the initial drop in the diffusion coefficient ratio more closely parallels the macroscopic viscosity. At these concentrations, the RTILs would be expected to be either separated ions or ion pairs, more closely mimicking typical salt solutions. As a result, as low concentrations, the Stokes-Einstein relationship appears to be followed. More study though is necessary on this point as few data points are available.

3.2. Spectroelectrochemistry of C_{60}

The spectroelectrochemistry of C_{60} in benzonitrile and mixed RTIL/benzonitrile solutions was done. The spectra for each species were determined using evolving factor analysis of the forward scan. The results for the spectroelectrochemistry in benzonitrile are consistent with the work of Dubois et al. with λ_{max} values of 332 (3 3 0), 338 (3 3 9), 340 (34 0) and 340 nm for C_{60}, C_{60}^{-}, C_{60}^{2-} and C_{60}^{3-}, respectively (number in parentheses are the value of Dubois et al. in methylene chloride). Each reduction was well separated enough to determine each spectra. As described in the Experimental section, all solutions were prepared in a glovebox under an argon atmosphere and water was removed prior to solution preparation. There was no evidence in the C_{60} spectrum of the formation of $C_{60}O$, as was observed by Xiao et al., in their study of C_{60} films under different solution conditions. With each reduction, the spectra became broader with a new shoulder appearing around 380 nm. Spectroelectrochemical reduction of C_{60} in 20% $BMImPF_6$/benzonitrile showed very similar behavior (Fig. 8) with some small differences, and the individual spectra were obtained using evolving factor analysis. The spectra for C_{60} in benzonitrile and 20% $BMImPF_6$ were nearly identical. This is consistent with the low solubility of C_{60} in RTILs, indicating poor solvation of C_{60} itself by the RTIL. Differences were observed though for the reduction products, as shown in Fig. 8. The bands for the 20% RTIL mixtures were generally sharper than for pure benzonitrile. The λ_{max} values were blue shifted from pure benzonitrile: C_{60}^{-}: 334 (3 3 8),

C_{60}^{2-}: 336 (3 4 0), C_{60}^{3-}: 338 (3 4 0) nm (values in parentheses are for pure benzonitrile). These small shifts are difficult to interpret, but the changes in the shape of the 340 nm band are indications of significant interactions between the RTIL and the anionic C_{60} species. There was an increase in absorbance between 700–800 nm, which was related to the near infrared band around 800 nm. This band nearly disappears in the presence of the RTIL, and was related to changes in the near infrared spectrum of C_{60}^{3-} (see below). It is difficult to interpret these changes on the molecular level, but it is consistent with a strong interaction between the fullerides and the RTIL.As discussed in the Introduction, the near infrared spectroscopy provides more characteristic identification of the different oxidation states of the fullerides. The near infrared spectra of C_{60}^{-} and C_{60}^{2-} in benzonitrile and benzonitrile/$AmNTf_2$ are quite similar, showing minimal spectral changes in the presence of the RTIL (Supplementary Information Figure S7). On the other hand, the presence of the RTIL led to measurable changes in the near infrared spectrum of C_{60}^{3-} (Fig. 9). The shifts in the λ_{max} values were relatively small (956 to 952 nm, 788 to 784 nm, 878 nm band became a shoulder), but the molar absorptivities changed significantly with 952 nm band having the strongest absorbance, as compared to the 788 nm band in benzonitrile alone. The 1367 nm band appears to be blue-shifted, but the overlap with the solvent/electrolyte makes it difficult to measure accurately. The spectroelectrochemical results are consistent with the voltammetric data. The strongest interaction in the voltammetry was observed between the RTIL nanodomains and C_{60}^{3-}. Similarly, the most significant changes in the visible/near infrared spectra are observed with the C_{60}^{3-} spectrum.

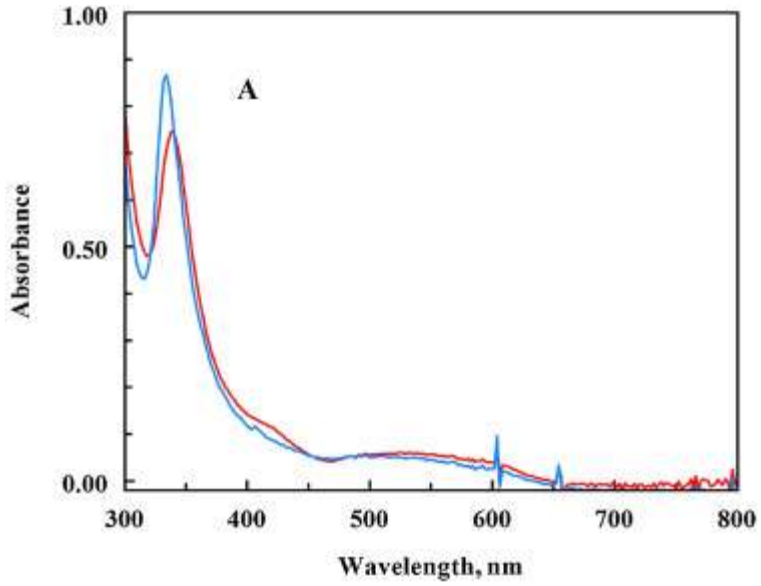

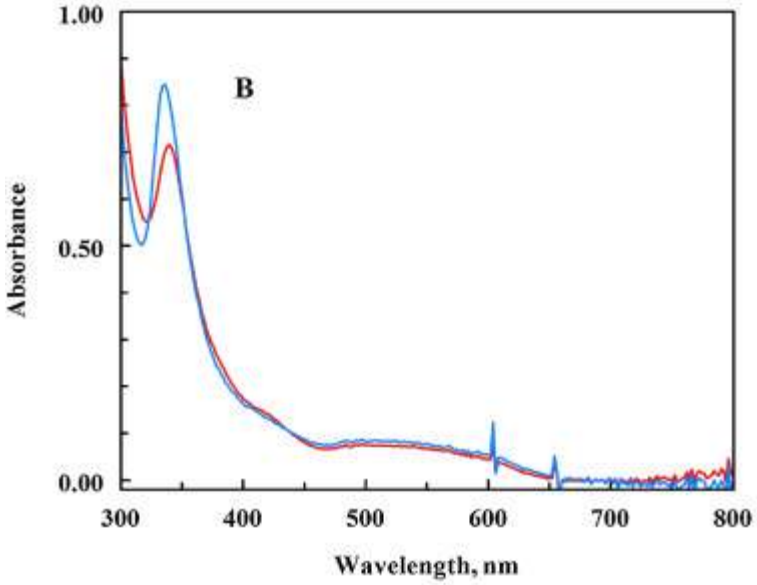

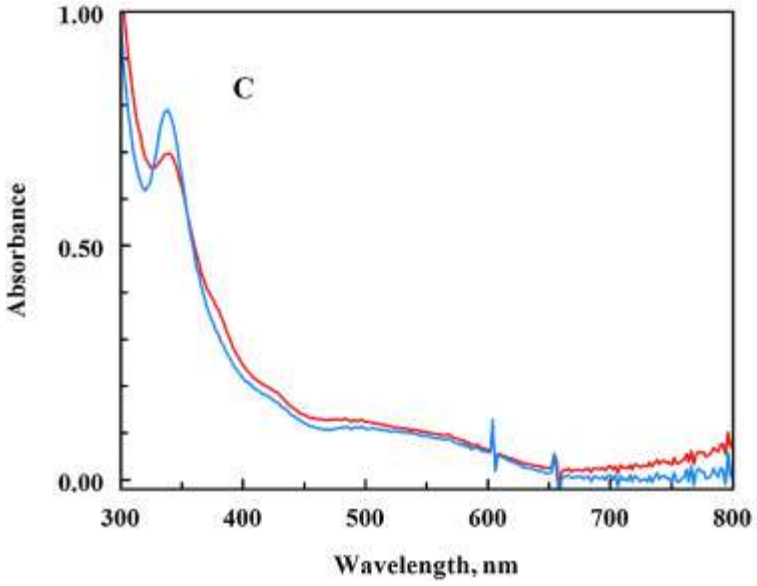

Fig. 8. Spectroelectrochemistry for anionic C_{60} species. A) C_{60}^{-}, B) C_{60}^{2-}, C) C_{60}^{3-}. Red lines correspond to benzonitrile, blue lines to 20% $BMImPF_6$/benzonitrile. Benzonitrile contained 0.10 M TBAP. (For interpretation of the references to color in this figure legend, the reader is referred to the web version of this article.)

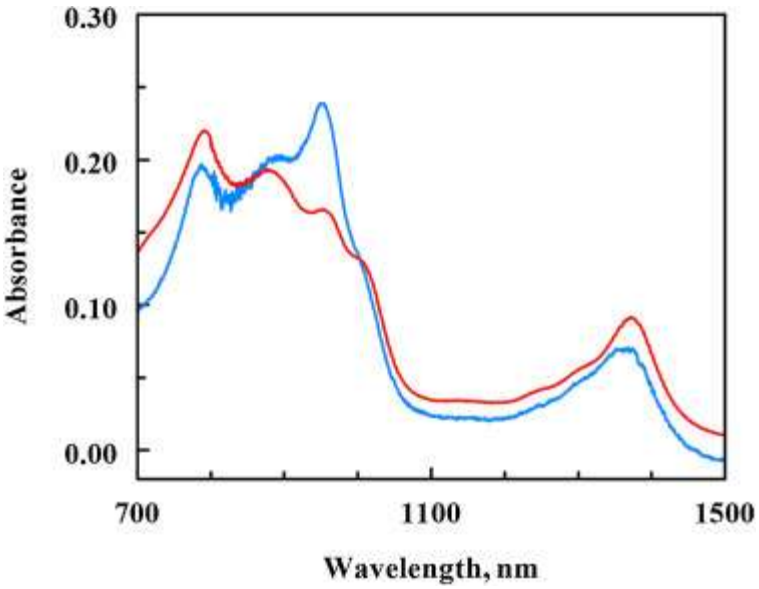

Fig. 9. Near infrared spectra of C_{60}^{3-}, as obtained using spectroelectrochemistry at −1.8 V vs $Ag/AgNO_3$. Red lines are from the spectroelectrochemistry of C_{60} in benzonitrile/0.10 M TBAP; blue lines are from the spectroelectrochemistry of C_{60} in benzonitrile/33% $AmNTf_2$. The band at 1384 nm is due to the benzonitrile/TBAP solution. (For interpretation of the references to color in this figure legend, the reader is referred to the web version of this article.)

Shimizu et al. described the nano-segregated structure on ionic liquids as four regimes, as discussed in the Introduction. Using their molecular dynamic (MD) simulation of $BMImNTf_2$/acetonitrile as a model, the formation of filamentous aggregates would occur between 10–20% of the RTIL in molecular solvents (mole fraction, χ, about 0.06). The exact number will vary of course with the physical properties of the molecular solvent and the RTIL. At 40% RTIL, the mixture is expected to move into the intermediate domain where the molecular solvent has permeated into the ionic liquid, breaking some of the ionic interactions. The MD snapshot shows an ionic liquid with islands of molecular solvent. It is also in this regime that fullerene ceases to be soluble in the benzonitrile/RTIL mixtures. Thus, in this study of fullerene, we are able to span all four regimes from neat ionic liquid (for fulleride in $AmNTf_2$ to separated ions in 1–2% RTIL, or 0.03 to 0.06 M).

The effect of aggregation and RTIL nanodomains is reflected in the comparison of the $E_{1/2}$shifts observed with added salts. For non-RTIL salts, the shifts in the $E_{1/2}$ values follow classical ion pairing equilibria. For comparison with the regimes described above, the range from 0–0.5 M RTIL corresponds to χ = 0 to 0.06. The lowest concentrations are clearly in the separated ion regime, but the higher concentration is in the regime where nanosegregated filamentous structures are expected to be observed. For non-RTIL salts, dianionic and trianionic fullerides formed successive ion pairs with one, two or three cations of TBA^+ and THA^+, depending upon the charge on the fulleride. The large planar cation, $BMIm^+$, of the non-RTIL salt coordinated weakly or not at all with the fullerides. On the other hand, RTILs that contained $BMIm^+$ strongly interacted with fullerides, especially C_{60}^{3-}. Unlike the TBA^+cation, the shift in the $E_{1/2}$ in the presence of the RTIL showed no evidence of successive ion pairs (one, two, three cations), but the shift was related to the concentration of the RTIL to the first power, as if the RTIL interacted as a single species. In addition, the formation constant was much larger than the $K_{IP,1}$ of the non-RTIL salts. This is most consistent with the interaction of fullerides with the nano-aggregates (nanodomains) of the RTIL which contain several points of coulombic interaction with the fulleride. While $BMIm^+$ (from the chloride salt) interacted weakly with fullerides, $BMIm^+$ aggregates can interact strongly with the fulleride because of the presence of several $BMIm^+$ ions in close proximity.

The second indication of the effect of nanodomains of RTILs in molecular solvents is the variation in the $\Delta E_{12}°$ and $\Delta E_{23}°$ values with Gutmann AN. The use of the difference between redox potential minimizes the effect of reference potential on the measure potential. At low concentration of the RTIL, the addition of cations with larger acceptor numbers than the solvent will stabilize the fullerides better than the molecular solvent itself. As a result, the $\Delta E°$ values follow the overall Gutmann AN of the solution (Fig. 4). As the aggregates grew, the fullerides (especially C_{60}^{3-}) began to be incorporated into the RTIL nanodomains. In this way, they were exposed to a predominately RTIL environment, providing a greater stabilization of the fulleride. This can be seen in Fig. 4 where the $\Delta E°$ values deviate significantly from the trendline at higher concentrations of the RTIL. This deviation occurs

when the RTIL/molecular solvent is expected to move into the 3rd regime, where the RTIL is essentially continuous in the solution with islands of molecular solvent (see Fig. 8 of Reference 2). This deviation is most prominent for the $AmNTf_2$ RTIL, where the flexibility of the Am^+ ion enables it to interact more strongly with the spherical fulleride. This would allow for an easier entry of the anionic substrate in the RTIL domains of $AmNTf_2$ as compared to $BMImPF_6$ or $BMImBF_4$. This can be particularly observed in the deviation of the $AmNTf_2$data from the trendline in Fig. 4B for high concentrations of the RTIL.

The third indication of the influence of the RTIL nanodomains is the spectra of the fullerides in the presence of the RTIL. The spectra of the less highly charged fullerides (C_{60}^- and C_{60}^{2-}) are not strongly influenced by the presence of the RTIL. On the other hand, the most highly charged fulleride studied (C_{60}^{3-}) showed changes in the visible spectrum, and more significant changes in the near infrared spectrum. Voltammetric data showed that the C_{60}^{3-}interacted most strongly with the RTIL nanodomains (Table 1).

The fourth indication of the formation of the nanodomains is the relationship between the diffusion coefficient of C_{60} and the overall viscosity of the mixed solvent. While the viscosity of the mixed solvent dropped rapidly with the addition of the RTIL, the diffusion coefficient decreased modestly. This would be consistent with molecular solvent domains between the RTIL nanodomains. If the RTIL mixed homogeneously with the solvent, the diffusion coefficient should be inversely proportional to the solution viscosity. While RTILs generally follow the Stokes-Einstein equation, significant deviations have been observed under some conditions. Brooks and Doherty reported a concentration-dependent diffusion coefficient for ferrocene in $BMImNTf_2$. A smaller but significant increase in the diffusion coefficient was also observed for ferrocene in $BMImBF_4$. Shiddiky et al. have also observed increases in diffusion coefficients due to the addition of other solutes. In the above cited works, they excluded other sources of the increase in diffusion coefficients such as the Dahms Ruff effects, migration transport and changes in viscosity. The most likely source of these diffusion coefficient changes are subtle changes in the RTIL structure due to interaction of the neutral or charged solutes with the RTIL aggregates that are present in pure RTILs. In our case, the

enhanced diffusion is approached from the opposite direction: addition of RTIL to a molecular solvent. If aggregation of RTIL into nanodomains occurs, the overall macroscopic viscosity will decrease in a predictable manner, but the microstructure environment that the solute (C_{60}) encounters may be more fluid due to the aggregation. This trend is consistent with the filamentous, rather than micellar, structure of the RTILs in molecular solvent rich mixtures. The filamentous structure would provide a more tortuous path to the electrode surface. We are in the process of investigating this effect with other solutes and RTILs. In this case, the insolubility of C_{60} in the RTIL domains (as indicated by its insolubility in the RTIL itself) forces the solute into the molecular solvent channels. As the concentration of the RTIL increases, the diffusion coefficient returned to the value expected based on the Stokes-Einstein relationship, before the fullerene eventually precipitating due to its insolubility in the RTIL. This is reasonable in that the mixtures has moved into the regime where the molecular solvent has percolated into an essentially RTIL solution.

4. Conclusions

The overall results show that the formation of aggregates of RTIL nanodomains within molecular solvent solutions have significant effects on the voltammetry of fullerene. The voltammetry was consistent with stabilization of the fullerides by interaction of the fullerides with RTIL nanodomains, not merely by classical ion pairing. The effect of RTILs in molecular solvent rich mixtures can be observed not only in the voltammetry, but also in the spectroscopy of the fullerides. Further studies are in progress on the effect of RTIL nanodomains on the molecular structure of the electroactive material.

Acknowledgments

We would like to acknowledge the Schmitt Foundation for fellowship support of this work.

References

K. Shimizu, M.F. CostaGomes, A.A.H. Pádua, L.P.N. Rebelo, J.N. Canon gia Lopes J. Mol. Structure, 946 (2010), p. 70

A.A.H. Pádua, M.F. Costa Gomes, J.N.A. Canongia Lopes Acc. Chem. Res., 40 (2007), p. 1087

D.R. Schreiber, M.C. De Lima, K.S. Pitzer J. Phys. Chem., 91 (1987), p. 4087

A. Atifi, M.D. Ryan Anal. Chem., 86 (2014), p. 6617

A. Atifi, M.D. Ryan Anal. Chem., 87 (2015), p. 12245

R.E. Haufler, J. Conceicao, L.P.F. Chibante, Y. Chai, N.E. Byrne, S. Flan agan, M.M. Haley, S.C. O'Brien, C. Pan, Z. Xiao, W.E. Billups, M. A. Ciufolini, R.H. Hauge, J.L. Margrave, L.J. Wilson, R.F. Curl, R. E.Smalley
J. Phys. Chem., 94 (1990), p. 8634

P.M. Allemand, A. Koch, F. Wudl, Y. Rubin, F. Diederich, M.M. Alvarez, S.J. Anz, R.L. Whetten
J. Am. Chem. Soc., 113 (1991), p. 1050

D. Dubois, K.M. Kadish, S. Flanagan, R.E. Haufler, L.P.F. Chibante, L.J. Wilson J. Am. Chem. Soc., 113 (1991), p. 4364

C.A. Reed, R.D. Bolskar Chem. Rev., 100 (2000), p. 1075

D. Dubois, K.M. Kadish, S. Flanagan, R.E. Haufler, L.P.F. Chibante, L.J. Wilson J. Am. Chem. Soc., 113 (1991), p. 7773

D. Xie, E. Perez-Codero, L. Echegoyen J. Am. Chem. Soc., 114 (1992), p. 3978

Y. Ohsawa, T. Saji Chem. Commun. (1992), p. 781

D. Dubois, G. Moninot, W. Kutner, M.T. Jones, K.M. Kadish
J. Phys. Chem., 96 (1992), p. 7137

J. Stinchcombe, A. Pénicaud, P. Bhyrappa, P.D.W. Boyd, C.A. Reed
J. Am. Chem. Soc., 115 (1993), p. 5212

P. Bhyrappa, P. Paul, J. Stinchcombe, P.D.W. Boyd, C.A. Reed
J. Am. Chem. Soc., 115 (1993), p. 11004

Y. Sun, C.A. Reed Chem. Commun. (1997), p. 747

M. Baumgarten, L. Gherghel Appl. Magn. Reson., 11 (1996), p. 171

M.A. Greaney, S.M. Gorun J. Phys. Chem., 95 (1991), p. 7142

G.A. Heath, J.E. McGrady, R.L. Martin J. Chem. Soc. Chem. Commun. (1992), p. 1272

T. Kato, T. Kodama, M. Oyama, S. Okazaki, T. Shida, T. Nakagawa, Y. Matsui, S. Suzuki, H. Shiromaru, K.Yamauchi, Y. Achiba
Chem. Phys. Lett., 186 (1991), p. 35

T. Kato Laser Chem., 14 (1994), p. 155

D.R. Lawson, D.L. Feldheim, C.A. Foss, P.K. Dorhout, C.M. Elliott, C.R. Martin, B. Parkinson

J. Electrochem. Soc., 139 (1992), pp. L68-L71

M.M. Khaled, R.T. Carlin, P.C. Trulove, G.R. Eaton, S.S. Eaton
J. Am. Chem. Soc., 116 (1994), p. 3465

P.C. Trulove, R.T. Carlin, G.R. Eaton, S.S. Eaton J. Am. Chem. Soc., 117 (1995), p. 6265

I. Noviandri, R.D. Bolskar, P.A. Lay, C.A. Reed J. Phys. Chem. B, 101 (1997), p. 6350

I. Noviandri, K.N. Brown, D.S. Fleming, P.T. Gulyas, P.A. Lay, A.F. Masters, L. Phillips J. Phys. Chem. B, 103 (1999), p. 6713

C. Jehoulet, A.J. Bard, F. Wudl J. Am. Chem. Soc., 113 (1991), p. 5456

W. Adamiak, M. Opallo J. Electroanal. Chem., 643 (2010), p. 82

N.W. Duffy, A.M. Bond Electrochem. Commun., 8 (2006), p. 892

H. Ueda, K. Nishiyama, S. Yoshimoto Electrochem. Commun., 43 (2014), p. 102

P. Damlin, C. Kvarnstroem, A. Ivaska J. Electroanal. Chem., 590 (2006), p. 190

B.A. Rosen, A. SalehiKhojin, M.R. Thorson, W. Zhu, D.T. Whipple, P.J.A Kenis, R.I. Masel Science, 334 (2011), p. 643

D. Niu, H. Wang, H. Li, Z. Wu, X. Zhang Electrochim. Acta, 158 (2015), p. 138

J. Shi, F. Shi, N. Song, J.X. Liu, X.K. Yang, Y.J. Jia, Z.W. Xiao, P. Du J. Power Sources, 259 (2014), p. 50

L. Sun, G.K. Ramesha, P.V. Kamat, J.F. Brennecke Langmuir, 30 (2014), p. 6302

A.E. Visser, R.P. Swatloski, W.M. Reichert, J.H. Davis Jr., R.D. Rogers, R. Mayton, S. Sheff, A. Wierzbicki Chem. Commun. (2001), p. 135

E.D. Bates, R.D. Mayton, I. Ntai, J.H. Davis Jr. J. Am. Chem. Soc., 124 (2002), p. 926

M. Schmeisser, P. Illner, R. Puchta, A. Zahl, R. van Eldik Chem.- Eur. J., 18 (10969) (2012), p. S10969

W. Li, Z. Zhang, J. Zhang, B. Han, B. Wang, M. Hou, Y. Xie Fluid Phase Equilib., 248 (2006), p. 211

M.J. Frisch, G.W. Trucks, H.B. Schlegel, G.E. Scuseria, M.A. Robb, J.R. Cheeseman, G. Scalmani, B.Barone, B. Mennucci, G.A. Petersso n, H. Natatsuji, M. Caricota, X. Li, H.P. Hratchian, A.F. Izmaylov, J.Bloino, G. Zheng, J.L. Sonnenberg, M. Hada, M. Ehara, K. Toy ota, R. Fukuda, J. Hasegawa, M. Ishida, T.Nakajima, Y. Honda,

O. Kitao, H. Nakai, T. Vreven, J.A. Montgomery Jr., J.E. Peralta, F. Ogliaro, M.Bearpark, J.J. Heyd, E. Brothers, K.N. Kudin, V.N. Staroverov, R. Kobayashi, J. Normand, K.Raghavachari, A. Rend ell, J.C. Burant, S.S. Iyengar, J. Tomasi, M. Cossi, N. Rega, N.J. Millam, M. Klene, J.E. Knox, J.B. Cross, V. Bakken, C. Adamo, J. Jaramillo, R. Gomperts, R.E. Stratmann, O. Yazyev, A.J.Austin, R. Cammi, C. Pomelli, J.W. Ochterski, R.L. Martin, K. Morokuma, V.G. Zakrzewski, G.A. Voth, P.Salvador, J.J. Dannenberg, S. Da pprich, A.D. Daniels, Ö.Farkas, J.B. Foresman, J.V. Ortiz, J.Ciosl owski, D.J. Fox**Gaussian D.09** Gaussian, Inc., Wallingford, CT (2009)

M.W. Lehmann, P. Singh, D.H. Evans J. Electroanal. Chem., 549 (2003), p. 137

A.J. Fry Electrochem. Commun., 7 (2005), p. 602

V.A. Nikitina, F. Gruber, M. Jansen, G.A. Tsirlina Electrochim. Acta, 103 (2013), p. 243

N.A. Macías-Ruvalcaba, D.H. Evans J. Phys. Chem. B, 109 (2005), p. 14642

A.J. Fry J. Org. Chem., 80 (2015), p. 3758

A. Fry Electrochem. Commun., 35 (2013), p. 88

V.A. Nikitina, R.R. Nazmutdinov, G.A. Tsirlina J. Phys. Chem. B, 115 (2011), p. 668

E.I. Rogers, D.S. Silvester, D.L. Poole, L. Aldous, C. Hardacre, R.G. Co mptonJ. Phys. Chem. C, 112 (2008), p. 2729

M.C. Lagunas, W.R. Pitner, J.-A. van den Berg, K.R. Seddon ACS Symp. Ser., 856 (2003), p. 421

J.S. Long, D.S. Silvester, A.S. Barnes, N.V. Rees, L. Aldous, C. Hardacr e, R.G. Compton J. Phys. Chem. C, 112 (2008), p. 6993

X. Zhang, H. Yang, A.J. Bard J. Am. Chem. Soc., 109 (1987), p. 1916

A.D. Clegg, N.V. Rees, O.V. Klymenko, B.A. Coles, R.G. Compton J. Am. Chem. Soc., 126 (2004), p. 6185

M.A. Vorotyntsev, V.A. Zinovyeva, M. Picquet Electrochim. Acta, 55 (2010), p. 5063

D.Y. Kim, J.C. Yang, H.W. Kim, G.M. Swain Electrochim. Acta, 94 (2013), p. 49

O.N. Kalugin, I.V. Voroshylova, A.V. Riabchunova, E.V. Lukinova, V.V. Chaban Electrochim. Acta, 105 (2013), p. 188

K.R. Seddon, A. Stark, M.J. Torres Pure Appl. Chem., 72 (2000), p. 2275

C.S. Consorti, P.A.Z. Suarez, R.F. deSouza, R.A. Burrow, D.H. Farrar, A.J. Lough, W. Loh, L.H.M. Da Silva, J. Dupont J. Phys. Chem. B, 109 (2005), p. 4341

J. Dupont, P.A.Z. Suarez, R.F. de Souza, R.A. Burrow, J.P. Kintzinger Chem. Eur. J., 6 (2000), p. 2377

A. Mele, C.D. Tran, S.H. De Paoli Lacerda Angew. Chem. Int. Ed., 42 (2003), p. 4364

A. Atifi, K. Czarnecki, H. Mountacer, M.D. Ryan Environ. Sci. Technol., 47 (2013), p. 8650

R.L. Keesey, M.D. Ryan Anal. Chem., 71 (1999), p. 1744

L. Xiao, G.G. Wildgoose, A. Crossley, R.G. Compton Sens. Actuators B, 138 (2009), p. 397

C.A. Brooks, A.P. Doherty Electrochem. Commun., 6 (2004), p. 867

S. Eisele, M. Schwarz, B. Speiser, C. Tittel Electrochim. Acta, 51 (2006), p. 5304

M.J.A. Shiddiky, A.A.J. Torriero, C. Zhao, I. Burgar, G. Kennedy, A.M. Bond J. Am. Chem. Soc., 131 (2009), p. 7976

M.J.A. Shiddiky, A.A.J. Torriero, J.M. Reyna-Gonzalez, A.M. Bond Anal. Chem., 82 (2010), p. 1680